Synaptic scaling rule preserves excitatory–inhibitory balance and salient neuronal network dynamics

Jérémie Barral[1] & Alex D Reyes[1]

The balance between excitation and inhibition (E–I balance) is maintained across brain regions though the network size, strength and number of synaptic connections, and connection architecture may vary substantially. We use a culture preparation to examine the homeostatic synaptic scaling rules that produce E–I balance and *in vivo*-like activity. We show that synaptic strength scales with the number of connections K as $\sim 1/\sqrt{K}$, close to the ideal theoretical value. Using optogenetic techniques, we delivered spatiotemporally patterned stimuli to neurons and confirmed key theoretical predictions: E–I balance is maintained, active decorrelation occurs and the spiking correlation increases with firing rate. Moreover, the trial-to-trial response variability decreased during stimulation, as observed *in vivo*. These results—obtained in generic cultures, predicted by theory and observed in the intact brain—suggest that the synaptic scaling rule and resultant dynamics are emergent properties of networks in general.

The firing dynamics of neural networks depend on the overall balance between excitation (E) and inhibition (I). Maintaining a balance of E and I inputs to neurons is crucial for coding[1], and severe imbalances can lead to neuropathologies[2–6]. The balanced state, characterized by neuronal activities that are neither completely silent nor saturated[7,8], exists in a wide range of networks with different configurations. The size, connection architecture, synaptic dynamics and strength, and intrinsic properties of E and I neurons vary widely across brain regions[9–11] and may change during development[12–15] and learning[16]. The presence of the balanced state under these different conditions suggests that potentially many network variables are adjusted homeostatically to maintain E–I balance and functional network dynamics.

Determining the homeostatic rules that lead to balance is difficult given the complexity of cortical circuits. One approach is to reduce the number of variables and use well-established mean-field techniques adapted from statistical mechanics to examine general network properties analytically[7,8,17]. Rather than incorporating as many of the experimentally determined variables as possible[18], only a few key parameters of the network are considered: the number (N) of E and I neurons, the strength (J) and number (K) of presynaptic connections per neuron, and the connection probability (P_c) between cells. For mathematical rigor, mean-field theories are developed in the limit of infinite network size and assume statistical independence between the variables. The network behavior depends critically on how J, K, P_c and N scale with respect to each other. Expressions for the mean and variance of the network-generated synaptic input and conditions to achieve E–I balance can be derived readily (see **Supplementary Math Note**). In this framework, general properties such as the firing rate or the correlation between neurons can be analytically predicted from network properties[7,8,17]. Ideally, any scaling scheme should not only achieve balance but also reproduce the salient features of *in vivo* activity and be constrained by experimentally determined parameters.

Under the constraint that the highly irregular firing of *in vivo* neurons be preserved[19–21], one scheme[7,8] requires that J scales with the number of connections K as $1/\sqrt{K}$. This scaling ensures that the fluctuations or variance (σ^2) in the synaptic input (σ^2 is proportional to $K \cdot J^2$; **Supplementary Math Note**) do not depend on the number of connections (σ^2 proportional to $K \cdot (1/\sqrt{K})^2 = $ constant). Fluctuations cause stochastic threshold crossings and hence irregular firing. Note that if, instead, J scales as $1/K$, the variance vanishes with increasing K. The balanced state is achieved provided that the mean excitatory synaptic input, E (composed of recurrent and external drive to the network), is equal in magnitude to the mean inhibitory synaptic input, I, so that the composite synaptic input (E – I) is close to rheobase (**Supplementary Math Note**).

Another constraint is that correlation in the firing of neurons must be low. Low correlation is crucial for ensuring statistical independence of variables required for mean-field[7,8,17] and for efficient coding of firing rate information under some circumstances[22]. To maintain low spiking correlations, one possibility is to set K to be large but much smaller than N ($1 \ll K \ll N$) by, for example, defining K to be a constant or to increase at a very slow rate with N. Under this condition, the probability P_c ($= K/N$) that neurons are connected is low (a 'sparsely connected' network[7,8,17]); correlations are reduced because the probability that two neurons receive common inputs ($= P_c^2$) is also small. However, estimates of the connection density of local cortical networks suggest that wiring is not sparse, especially when considering E–I wiring[14,18,23–29]. Nevertheless, correlations can also be small in networks where K increases proportionally with N, such that P_c is nonvanishing (a 'densely connected' network). Although dense connectivity induces positive correlations between isolated E inputs and between isolated I inputs to neurons, correlations in both the composite synaptic input and spiking are reduced because the E and I inputs covary in time (track each other) and cancel. Moreover, the correlation is predicted to decrease with network size[30]. In addition

to network parameters, spiking correlation is also affected by correlations in the external drive to the network[30] and by the firing rate of neurons[31].

A shortcoming of the reduced approach is that many of the simplifying assumptions needed for mathematical tractability appear far from physiological parameters. The $1/\sqrt{K}$ scaling rule and the relations between the variables were derived based not on biological principles but rather based on the fact that the model reproduced *in vivo*-like activity. Furthermore, the idealized network differs substantially from biological networks, in which K and N are finite, neurons have diverse membrane and firing properties, P_c varies with distance and cell type, and J exhibits time-dependent depression or facilitation.

Here, we use a culture preparation in which N can be systematically varied and K, J and P_c can be measured accurately. To determine whether the scaling results in E–I balance, high spiking variability and low correlations, we drive the network with specified spatiotemporal patterns using optogenetic stimulation. Using a variety of stimuli delivered under various conditions, we test whether the results hold under conditions different from the ideal theoretical limits and whether the network can accommodate other network behaviors not explicitly predicted by the theories.

RESULTS

Intrinsic and network properties of cortical cultures

To confirm that the properties of cortical neurons grown in the glia-free cultures were similar to those of neurons in acute slices, we characterized the intrinsic and synaptic properties of neurons by performing paired whole-cell recordings ($n = 491$ cells, 1,080 tested connections in 131 preparations). A neuron was classified as excitatory or inhibitory based on whether suprathreshold stimulation evoked depolarizing or hyperpolarizing responses in its postsynaptic target (**Fig. 1a**). Approximately 23% of the neurons in culture were inhibitory, consistent with estimates in cortical slices[27] and in cultures[32,33]. By 14 days *in vitro* (DIV), the resting membrane potential, the input resistance and the membrane capacitance stabilized. They remained constant for at least 30 DIV (**Supplementary Fig. 1** and **Supplementary Table 1**) and were similar to those measured in cortical slices[15,24,27]. The density did not change significantly with DIV for the range examined (**Supplementary Fig. 1**)[33].

As in *in vitro* slices of cortex[14,24], the connection probability between neurons decreased with distance, following a Gaussian profile (**Fig. 1b**). Organizational principles seemed similar to those measured in cortical slices ($P_{E\rightarrow E} \sim 0.2$, $P_{E\rightarrow I} = 0.3$–0.6, $P_{I\rightarrow E} = 0.4$–0.7 and $P_{I\rightarrow I} = 0.3$–0.7 for reported values[14,18,23–29]) with lower peak probability between E cells ($P_{E\rightarrow E} = 0.38$) than between E and I ($P_{E\rightarrow I} = 0.59$ and $P_{I\rightarrow E} = 0.64$) or between I cells ($P_{I\rightarrow I} = 0.59$) (**Supplementary Fig. 2** and **Supplementary Table 2**). However, the spatial profiles in this two-dimensional network were wide, with characteristic connection lengths of about 600 μm as compared to 100–200 μm in cortical slices[24,25,28,29].

To examine how the profile of connections varied with network size, we pooled data according to densities. The area under the connection profile P_c did not change substantially with density (**Fig. 1b,c** and **Supplementary Fig. 2g**). For each density, we estimated the total number (E + I; **Fig. 1c**) of presynaptic inputs (K) to a neuron by integrating the probability profiles over space (**Fig. 1c** and Online Methods), which provided a calibration curve relating the expected number of connections as a function of density. This allowed us to determine that K increased linearly with density, D (**Fig. 1c**; fit: $K = 0.82 \cdot D$, $R^2 = 0.995$), indicating that cortical neurons in culture form densely connected networks.

Scaling of synaptic strength with network size

The amplitudes of E and I postsynaptic potentials (EPSPs and IPSPs) decreased with density (**Fig. 1a**). At low densities (<100 neurons per mm^2), the unitary EPSP and IPSP amplitudes were 4.3 ± 1.4 mV and -3.8 ± 1.7 mV (mean ± s.d.), respectively, while at high densities (>300 neurons per mm^2), the values were 1.3 ± 1.1 mV and -1.4 ± 1.6 mV, consistent with previous results[34,35]. Using a general linear model, we determined that the amplitudes did not vary significantly with neuron type, DIV, distance or intrinsic properties (**Supplementary Table 3**).

Plotting the postsynaptic potential (PSP) amplitudes versus the expected number of connections K shows that the strengths J of both E and I synapses scale with K with an inverse power law (**Fig. 1d**). Fitting the combined E–I data in log–log scale (PSP amplitudes are log-normally distributed; **Supplementary Fig. 3**) gives an exponent of -0.59 (95% confidence interval: [-0.70:-0.47], $R^2 = 0.232$), comparable to the theoretically proposed $K^{-0.5}$ scaling[7,8]. Individual fits for unitary EPSPs and IPSPs have exponents of -0.60 and -0.52, respectively. Assuming that there are 1,500 connections per neuron in the intact cortex[18], this scaling (J (in mV) $= 32 \cdot K^{-0.59}$) predicts a PSP amplitude of $\sim$0.4 mV, well within an order of magnitude of the unitary PSP amplitudes ($\sim$0.1–0.5 mV) measured in cortical slices[14,18,24,28,36].
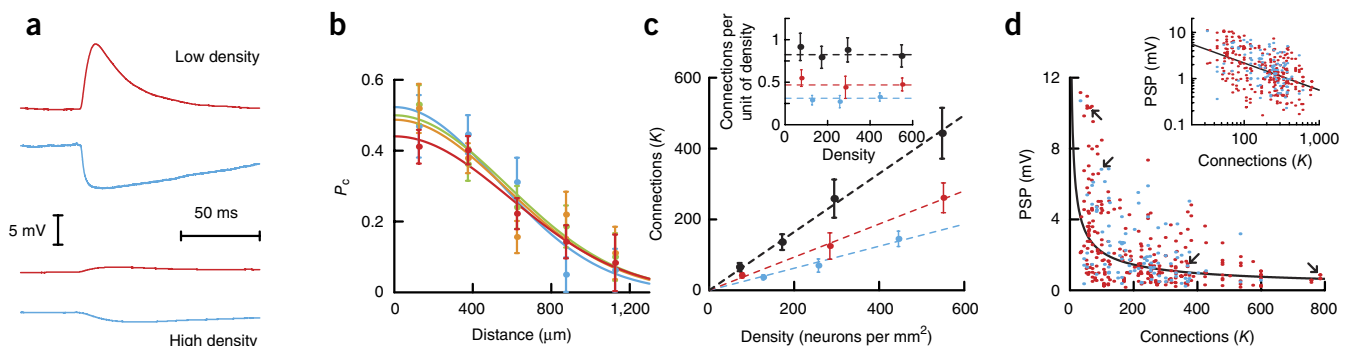
Figure 1 Synaptic scaling in networks of different sizes. (**a**) Representative E (red) and I (blue) PSPs in low and high density networks (arrows in **d**). (**b**) Connection probability vs. intersomatic distance in networks with average densities of 72 ($n = 194$ connections tested in 25 preparations, blue), 171 ($n = 329$ in 45, green), 294 ($n = 270$ in 32, orange), 548 ($n = 287$ in 29, red) neurons per mm^2. All connection types are pooled together. Data presented as mean ± s.e.m. (**c**) Number of connections (K) vs. density for E-to-E (red), I-to-E (blue) and total (black); s.d. calculated by bootstrapping data in **b**. Inset: integral of the connection probability profile over space. (**d**) Amplitudes (J) of unitary EPSPs (red, $n = 261$) and IPSPs (blue, $n = 99$) vs. K. Inset: data in log–log scales. Slope of linear fit is -0.59.
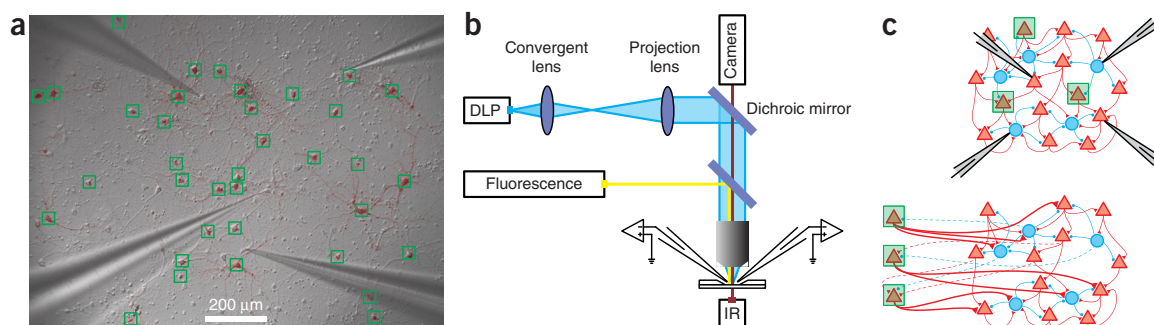
Figure 2 Optogenetic activation with spatiotemporal control. (**a**) Culture visualized with infrared differential interference contrast (IR-DIC) and fluorescent microscopy. (**b**) Using a digital light projector (DLP), the network was driven by delivering light pulses (green boxes in **a**) to neurons expressing ChR2 and a fluorescent tag (red). (**c**) The photostimulated ChR2 neurons (top) are effectively the external inputs to the network (bottom).

## Spiking dynamics of optogenetically driven network

To examine the spiking dynamics in the activated network, we stimulated a subset of neurons that expressed channelrhodopsin (ChR2) using a digital light processing projector (**Fig. 2a,b**). ChR2 (and a fluorescent tag) were expressed either only in E cells (transgenic lines) or nonspecifically in both E and I neurons (viral injection). Regions of interest (ROIs) covering the ChR2-expressing neurons were defined, and simultaneous cell-attached or whole-cell recordings established in 4 cells that either did not express ChR2 or whose somata did not overlap with the processes of neurons in the ROI (**Fig. 2a**). Stimuli were trains of random light pulses with input rates ν_{stim} ranging from 2–40 Hz (**Supplementary Fig. 4** and Online Methods). Because the light pulses are suprathreshold (**Supplementary Fig. 5**), the stimulated neurons approximate the external feedforward input to the network (**Fig. 2c**), although feedback from the network may generate additional, albeit weaker, activity in the stimulated neurons (**Supplementary Fig. 5**). Because the ChR2-expressing neurons were often close and had overlapping processes, each ROI may activate 1–4 neurons. Experiments in which ChR2 was expressed sparsely, so that neurons could be stimulated individually, produced qualitatively similar results (**Supplementary Fig. 6**). Note that spontaneous, network-wide bursts present in cultures were excluded from analyses (see "Data Analyses" section in Online Methods for rationale).

The responses in simultaneously recorded neurons in cell-attached (extracellular) mode are heterogeneous. Asynchronous stimulation of each ROI at 5 Hz increases firing rate above baseline activity in approximately 65% of nonstimulated neurons (106 out of 164 neurons in 44 cultures; **Fig. 3a,b**). Identical stimuli delivered to the network evoke robust activity in some cells (**Fig. 3a**) and little in others (**Supplementary Figs. 6** and **7**). Such variability likely occurs because a finite number of neurons within an enclosed area are stimulated, so local heterogeneity in the network circuitry produces differences in the average E and I inputs to each cell.

The evoked activity is consistent with several key theoretical predictions. First, the action potential firing is irregular: the Fano factor is ~1 and does not increase with the observation window (**Supplementary Fig. 8a**), indicating a near-Poisson process. Second, in accordance with the $1/\sqrt{K}$ scaling[7,8], the spiking variability does not decrease with increasing N (**Fig. 3c**). Third, the distribution of firing rates is long-tailed and approximately log-normal (**Fig. 3b** and **Supplementary Fig. 8b,c**), which is predicted by balance network theory[7,8,37] and is also in line with experimental results[38].

In addition, the network exhibits firing behaviors consistent with those documented in intact animals with natural stimuli. As observed *in vivo*[39] and predicted by theory[40], stimulation of the network

quenches variability in the number of spikes evoked over a time interval (**Fig. 3c**). The increase in firing rate during stimulation (**Fig. 3b**) is accompanied by a significant drop in the Fano factor across all densities (**Fig. 3c**). Examination of evoked activity during several sweeps of
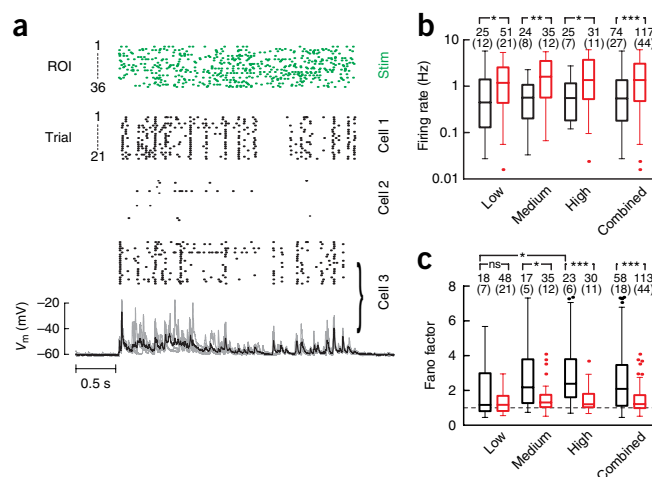
Figure 3 Evoked activity in the network. (**a**) Top: raster plots showing the spatiotemporally patterned stimuli (stim) over 36 ROIs. Middle: raster plots of evoked spikes (21 trials) in 3 cell-attached simultaneously recorded neurons. Bottom: whole-cell recordings from cell 3. Single trials (gray) superimposed on average (black). (**b**) Firing rate during spontaneous (black, average densities: low (L), 97; medium (M), 314; high (H), 744 neurons per mm²) and evoked (red; average densities: L, 188; M, 364; H, 653 neurons per mm²) activity in networks of different densities. Also shown is the data combined across densities. Statistical significance was assessed using Mann-Whitney *U*-test (the numbers of recorded neurons are shown below the statistical significance bars and numbers of cultures are shown in parentheses). No statistical difference was found between densities for a given condition. Spontaneous vs. evoked activity: $P = 0.0202$ (L), $P = 0.0021$ (M), $P = 0.0201$ (H), $P = 7.792 \times 10^{-6}$ (combined); for spontaneous activity: $P = 0.9124$ (L vs. M), $P = 0.6554$ (L vs. H), $P = 0.6383$ (M vs. H); for evoked activity: $P = 0.4111$ (L vs. M), $P = 0.5469$ (L vs. H), $P = 0.9385$ (M vs. H). (**c**) Fano factor of spike counts vs. density during spontaneous (black; average densities: L, 89; M, 289; H, 769 neurons per mm²) and evoked (red; average densities: L, 186; M, 364; H, 642 neurons per mm²) activity (number of trials was 10–30). Spontaneous vs. evoked activity: $P = 0.5032$ (L), $P = 0.0262$ (M), $P = 5.511 \times 10^{-4}$ (H), $P = 9.470 \times 10^{-5}$ (combined); for spontaneous activity: $P = 0.1094$ (L vs. M), $P = 0.0283$ (L vs. H), $P = 0.7427$ (M vs. H); for evoked activity: $P = 0.2868$ (L vs. M), $P = 0.2521$ (L vs. H), $P = 0.8693$ (M vs. H). Box plots indicate median and interquartile ranges; whiskers cover the full ranges of distributions and outliers are plotted individually. ns, not significant, *$P < 0.05$, **$P < 0.01$, ***$P < 0.001$.
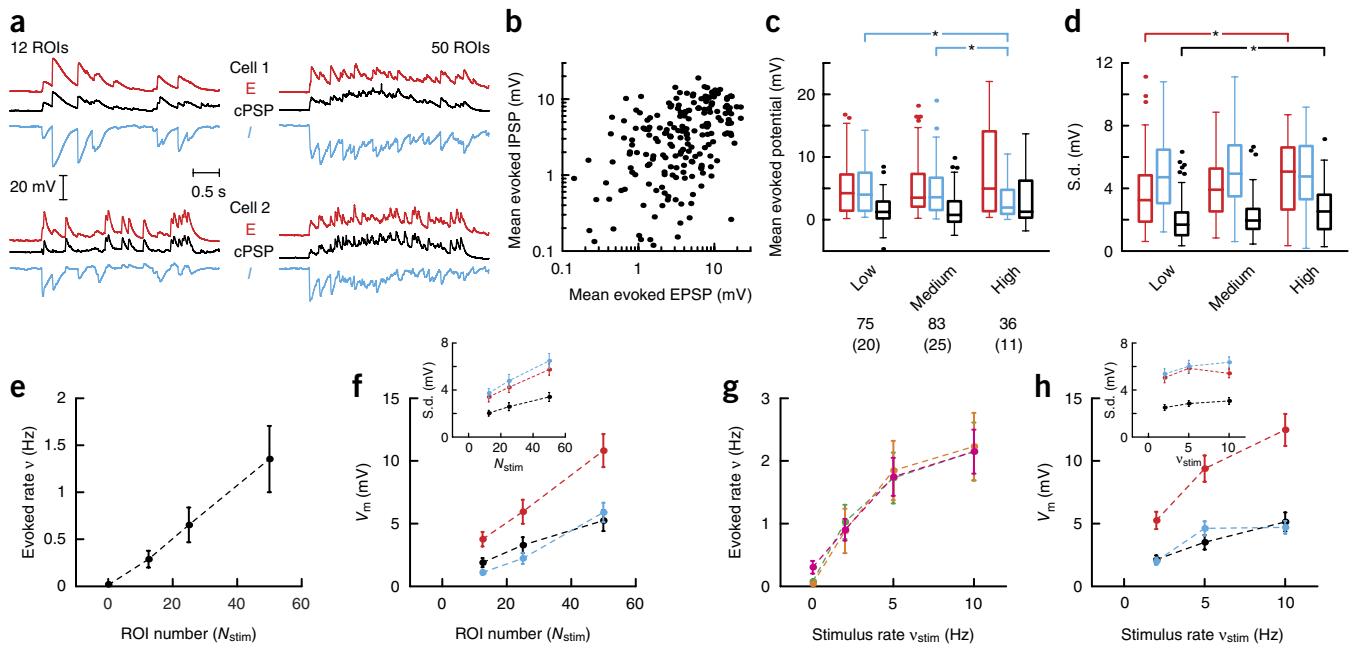
Figure 4 E–I balance in activated networks. (**a**) Trial-averaged isolated EPSPs (red), IPSPs (blue) and cPSPs (black) evoked with 12 and 50 ROIs, respectively, in 2 simultaneously recorded cells. (**b**) Plot of mean IPSP vs. mean EPSP. Data points ($n = 194$ cells in 56 preparations) are average magnitudes during optical stimulation (input rate $v_{stim} = 5$ Hz, stimulus correlation $C_{stim} = 0$) relative to baseline. IPSP magnitude increased linearly with IPSP magnitude (Pearson correlation: $r = 0.45$, $P = 3 \times 10^{-11}$). (**c**) Average membrane potential deviation from baseline during stimulation for EPSPs (red), IPSPs (blue) and cPSPs (black) in networks of different densities (low, 116; medium, 273; high, 544 neurons per mm^2). Only statistically significant tests using Mann-Whitney U-test are indicated. Neuron numbers are indicated below legends and numbers of preparations shown in brackets. Box plots indicate median and interquartile ranges, whiskers cover the full ranges of the distributions and outliers are plotted individually. *$P < 0.05$, **$P < 0.01$, ***$P < 0.001$. Low vs. medium density: $P = 0.7779$ (EPSP), $P = 0.3489$ (IPSP), $P = 0.2406$ (cPSP); low vs. high density: $P = 0.2914$ (EPSP), $P = 0.0127$ (IPSP), $P = 0.3660$ (cPSP); medium vs. high density: $P = 0.3622$ (EPSP), $P = 0.0469$ (IPSP), $P = 0.0637$ (cPSP). (**d**) As in **c** but for the s.d. of the membrane potential. Low vs. medium density: $P = 0.1835$ (EPSP), $P = 0.3507$ (IPSP), $P = 0.1077$ (cPSP); low vs. high density: $P = 0.0217$ (EPSP), $P = 0.8773$ (IPSP), $P = 0.0438$ (cPSP); medium vs. high density: $P = 0.0697$ (EPSP), $P = 0.6373$ (IPSP), $P = 0.2730$ (cPSP). (**e**) Firing rate vs. ROI number ($n = 16$ neurons in 5 preparations). (**f**) Average magnitude and s.d. (inset) of EPSPs (red), IPSPs (blue) and cPSPs (black) vs. ROI number ($n = 26$ neurons in 10 preparations). (**g**) Evoked firing rate vs. stimulus rate of light pulses delivered to each ROI in low ($n = 20$ neurons in 8 preparations, magenta), medium ($n = 22$ neurons in 6 preparations, green) and high ($n = 18$ in 6 preparations, orange) density networks. (**h**) Average magnitudes and s.d. (inset) of EPSPs (red), IPSPs (blue) and cPSPs (black) vs. stimulus rate ($n = 45$ neurons in 12 preparations). Data presented as mean ± s.e.m.

identical stimuli shows that the times of occurrences of some spikes are repeatable across trials (**Fig. 3a** and **Supplementary Figs. 6** and **7**). To characterize the underlying synaptic inputs, whole-cell recordings with the Na$^+$ channel blocker QX-314 present in the internal solution are established in the same cells (**Fig. 3a** and **Supplementary Fig. 7**). Large voltage transients coincide with the reliable extracellularly recorded spikes, while variable membrane potentials coincide with the unreliable spikes. These unreliable spikes are variable over repetitions of the identical stimulus and likely result from variability generated by the recurrent activity.

E–I balance in the activated network

To confirm that the E and I synaptic potentials evoked during stimulation are balanced, whole-cell current clamp recordings are established in 1–4 cells (**Fig. 4a**). At resting potential, the evoked compound PSP (cPSP) is a mixture of EPSPs and IPSPs. To isolate the EPSPs (IPSPs), the membrane potential is held at −80 mV (0 mV), near the reversal potential for IPSPs (EPSPs), and stimuli identical to those used to evoke cPSPs are delivered. Consistent with the balanced regime in *in vivo* data[41], the EPSPs (**Fig. 4a**) are countered by IPSPs of comparable amplitude, resulting in smaller cPSPs. Balance is achieved at the cellular level: the average evoked IPSPs and EPSPs to a single cell are linearly related (**Fig. 4b**), similar to *in vivo* findings[42].

The balanced regime is maintained irrespective of network size. The mean cPSP does not increase significantly with network density (despite the $\sqrt{K}$ term in equation 3 of **Supplementary Math Note**) because the E drive is matched by a comparably size I drive (**Fig. 4c**). In accordance with the $1/\sqrt{K}$ scaling of synaptic strength, the variability of EPSPs, IPSPs and cPSPs during stimulation does not decrease with density (**Fig. 4d**). This effect is maintained for both low and high numbers of stimulated neurons (**Fig. 4a**).

In the balanced regime, the mean firing rate of neurons should on the average be proportional to the magnitude of the external drive[7,8,30]. Increasing the number (N_{stim}) of ROIs causes a linear increase in the evoked rate (v) (**Fig. 4e**) and in the average (**Fig. 4a,f**) and standard deviation (**Fig. 4f**) of EPSPs, IPSPs and cPSPs. Similar observations are made when the rate of each ROI (v_{stim}; at constant N_{stim}) is increased (**Fig. 4g,h**). The apparent nonlinear relation becomes more linear (**Supplementary Fig. 9**) when v_{stim} is corrected for the frequency-dependent decline in the efficacy of ChR2 (**Supplementary Fig. 5**). Synaptic depression and/or firing rate adaptation may also contribute to the saturation. The firing rate gain (v/v_{stim}) is homeostatically maintained and does not change with density (**Figs. 3b** and **4g**; the mean drive is proportional to $N_{stim} \cdot J$ and is kept constant at each density by scaling N_{stim} by $\sqrt{density}$).
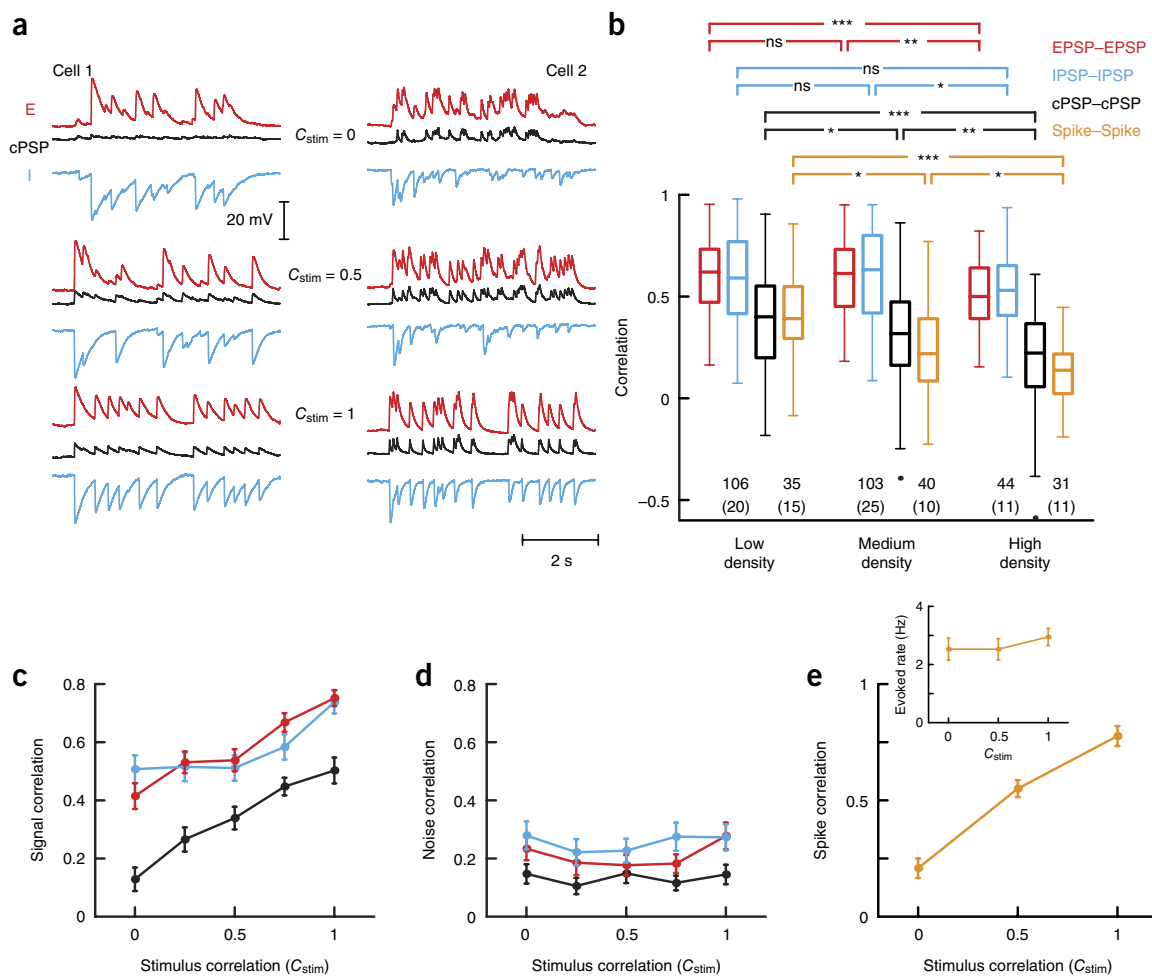
Figure 5 Correlations in activated networks. (**a**) Trial-averaged membrane potentials for 2 simultaneously recorded cells when the correlations between ROIs (C_{stim}) were 0 (top), 0.5 (middle), and 1 (bottom). Low vs. medium density: $P = 0.5744$ (EPSP), $P = 0.6830$ (IPSP), $P = 0.0307$ (cPSP), $P = 0.0117$ (spikes); low vs. high density: $P = 8.584 \times 10^{-4}$ (EPSP), $P = 0.0902$ (IPSP), $P = 6.174 \times 10^{-5}$ (cPSP), $P = 8.262 \times 10^{-6}$ (spikes); medium vs. high density: $P = 0.0044$ (EPSP), $P = 0.0315$ (IPSP), $P = 0.0078$ (cPSP), $P = 0.0272$ (spikes). (**b**) E (red), I (blue), cPSP (gray) and spike (orange) zero-lag correlation coefficient vs. density. Stimulus rate $v_{stim} = 5$ Hz and correlation $C_{stim} = 0$. For membrane potential, average densities were L: 116, M: 273, H: 544 neurons per mm^2 and for spikes average densities were L, 199; M, 374; H, 653 neurons per mm^2. Statistical significance was assessed using Mann-Whitney U-test. Numbers of neuronal pairs are indicated below whisker plots (box: median and interquartile range, whiskers: full range of the distribution; outliers are plotted individually) and numbers of preparations in brackets. ns, not significant, $*P < 0.05$, $**P < 0.01$, $***P < 0.001$. (**c,d**) Correlations between isolated EPSPs (red), isolated IPSPs (blue) and cPSPs (black) for signal (**c**) and noise (**d**) correlations ($n = 45$ pairs in 12 preparations). (**e**) Spike correlation vs. C_{stim} ($n = 28$ pairs in 8 preparations). Inset: corresponding evoked firing rate. Data are presented as mean ± s.e.m.

Spiking and membrane potential correlations in driven networks

Because the networks are densely connected ($K \propto N$ so that P_c is constant) with the $K^{-0.59}$ synaptic scaling, neurons share substantial and strong inputs from common sources, which would result in significant spiking correlation in the large N limit. However, correlations are reduced because E and I track and cancel each other[30,41,43]: during stimulation, the fluctuations in the isolated E inputs to neurons mirror those in I inputs (**Figs. 4a** and **5a**). A hallmark of E–I tracking is that the correlation between E inputs to two neurons and between isolated I inputs is larger than that between cPSPs. This is confirmed in simultaneously recorded pairs by cross-correlating the isolated EPSPs, isolated IPSPs and cPSPs (**Fig. 5a**). Similar results are obtained by cross-correlating the trial-averaged traces ('signal correlation') and by cross-correlating the individual traces after subtracting the averaged traces ('noise correlation'; **Supplementary Fig. 10**).

In the asynchronous state, the spiking correlation decreases with N due to improved E–I tracking[30]. As predicted, increasing the network density reduces both the correlations in spikes and cPSPs while E–E and I–I correlations remain high (**Fig. 5b**).

To confirm that E–I tracking attenuates correlations in the external drive[30], we systematically vary the correlation between the stimulated neurons. Correlations in the light stimuli are adjusted via the stimulus correlation parameter (C_{stim}) of the algorithm for generating pulse trains[31] (**Supplementary Fig. 4** and Online Methods). The time courses of both the EPSPs and IPSPs mirror each other and change in parallel with C_{stim} (**Fig. 5a** and **Supplementary Fig. 6**) to preserve both E–I balance (**Supplementary Fig. 11**) and tracking. The signal (**Fig. 5c**) and noise (**Fig. 5d**) correlations between cPSPs are substantially less than those between the isolated EPSPs or IPSPs. The noise correlation does not change with C_{stim}. The increase in signal correlation with C_{stim} reflects the fact that the tracking is not
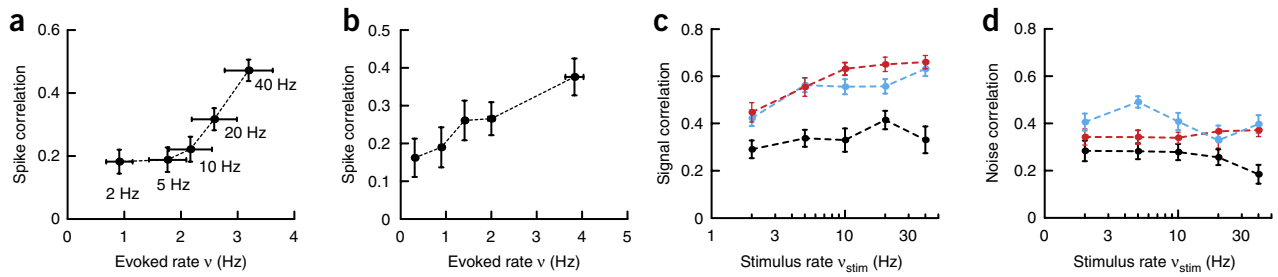
Figure 6 Relationship between rate and correlation. (**a**) Plot of spike correlation vs. geometric mean of the firing rates evoked by different stimulus rates v_{stim} ($n = 37$ pairs in 9 preparations). Numbers indicate v_{stim}. (**b**) Spike correlation vs. geometric mean of the firing rates (constant $v_{stim} = 5$Hz; data were pooled according to their mean firing rates; each data point represents ~21 pairs, in total 106 neuronal pairs in 44 preparations). (**c,d**) Signal (**c**) and noise (**d**) correlation vs. v_{stim} for EPSPs (red), IPSPs (blue) and cPSPs (black) ($n = 48$ neuronal pairs in 9 preparations; $C_{stim} = 0$; 30–60 ROIs). Data presented as mean ± s.e.m.

perfect. Because only E neurons are stimulated, there is a short delay between E and I, which prevents complete cancellation and becomes more apparent at high C_{stim}. The enhanced voltage transients in the cPSPs with increasing C_{stim} (**Fig. 5a**) result in more precise spiking and hence high spike correlations (**Fig. 5e**). Using cultures in which both E and I neurons are photoactivated simultaneously to eliminate the E–I delay reduces correlations in the cPSP and therefore in the spikes (**Supplementary Fig. 12**).

Finally, we confirm that spiking correlation covaries with the firing rate of the neurons due to the threshold nonlinearity in the neuronal transfer functions[31]. This relation between rate and correlation has been difficult to examine *in vivo* because recurrent synaptic inputs to neurons cannot be controlled. Therefore, the correlation in the synaptic input current, defined here as C_{in}, is not known, and an increase in the spiking correlation could simply be due to an increase in C_{in}. As predicted, increasing the stimulus rate (v_{stim}, as in **Fig. 4g**) increases both the firing rate and spiking correlations between neuron pairs (**Fig. 6a**). Similar results are obtained with v_{stim} fixed at 5 Hz, which produces a sufficiently broad range of firing rates for analyses (**Fig. 6b**). The increase in correlation is not accompanied by an increase in C_{in}: the signal (**Fig. 6c**) and noise (**Fig. 6d**) correlations in the subthreshold membrane potential (cPSP–cPSP) remain flat.

DISCUSSION

In summary, the data indicate that the $1/\sqrt{K}$ scaling rule predicted by theory occurs in a network of live neurons. This scaling ensures that E–I balance and network dynamics are homeostatically maintained in different size networks. The biological mechanism underlying the scaling is unknown but may be related to the network parameters as follows. To a first approximation, $J = s_b \cdot n_b$, where n_b is the number of boutons from a single presynaptic cell[18,29], each of which evokes a unitary response with magnitude s_b. The total number of boutons onto a cell is therefore $N_b = K \cdot n_b$ so that $J = s_b \cdot N_b/K$. In cultures, s_b (taken to be miniature EPSPs) is constant[35], suggesting that it is N_b that should increase as $\sqrt{K}$ to satisfy the $1/\sqrt{K}$ scaling.

Indeed, several lines of evidence suggest that the number of synaptic boutons per neuron increases with the number of neurons in the culture. Increasing the density eightfold decreases synaptic strength threefold but increases the number of dendritic spines twofold[35]. Similarly, increasing the network size tenfold while maintaining constant density weakens synaptic strength fourfold but increases the number of boutons twofold[34]. Altogether, these results suggest that the decreased synaptic strength in denser networks is mediated by a sublinear increase in the number of synaptic boutons. The underlying physiological and molecular mechanisms

are unknown but may be related to the homeostatic processes that regulate activity in culture[44] and *in vivo*[45]. In these cases, a combination of synaptic scaling and modification of intrinsic properties regulates the overall activity of the neuronal network in response to an experimental perturbation. In our experiments, activity level and variability, both of which are constant across density, may be the set point variables.

Two concerns are that the culture preparation does not fully replicate the *in vivo* circuitry and that the cellular and synaptic characteristics depend on the particular methodology[46,47]. Under the conditions of our experiments, the intrinsic properties of neurons and the projected PSP amplitudes calculated with the scaling rule are comparable to those measured in acute slices. Importantly, the evoked activity of the cultured neurons replicates several salient features of *in vivo* activity—irregular firing and stimulus-dependent decrease in trial-to-trial spiking variability[39], lognormal distribution of firing rate[38] and E–I tracking[41,42]—found in functionally diverse brain areas. Thus, cultures contain essential elements common to neuronal networks in general.

With unprecedented control of key experimental variables, we confirm the major predictions of seminal theories and show that they hold under conditions far from the asymptotic limits where K and N are large. Spike variability, the balanced regime and decorrelation by E–I tracking occurred even in low-density networks driven with spatially restricted, correlated external stimuli. Hence, highly simplified models, when backed by a strong theoretical framework, can be used to elucidate basic operating principles of networks.

METHODS

Methods, including statements of data availability and any associated accession codes and references, are available in the online version of the paper.

Note: Any Supplementary Information and Source Data files are available in the online version of the paper.

AUTHOR CONTRIBUTIONS
J.B. and A.D.R. designed the project. J.B. performed the experiments and analyzed the results. J.B. and A.D.R. wrote the manuscript.

COMPETING FINANCIAL INTERESTS
The authors declare no competing financial interests.

Reprints and permissions information is available online at http://www.nature.com/reprints/index.html.

1. Denève, S. & Machens, C.K. Efficient codes and balanced networks. *Nat. Neurosci.* **19**, 375–382 (2016).
2. Dichter, M.A. & Ayala, G.F. Cellular mechanisms of epilepsy: a status report. *Science* **237**, 157–164 (1987).
3. Trevelyan, A.J., Sussillo, D., Watson, B.O. & Yuste, R. Modular propagation of epileptiform activity: evidence for an inhibitory veto in neocortex. *J. Neurosci.* **26**, 12447–12455 (2006).
4. Yizhar, O. *et al.* Neocortical excitation/inhibition balance in information processing and social dysfunction. *Nature* **477**, 171–178 (2011).
5. Rubenstein, J.L. & Merzenich, M.M. Model of autism: increased ratio of excitation/inhibition in key neural systems. *Genes Brain Behav.* **2**, 255–267 (2003).
6. Lewis, D.A., Curley, A.A., Glausier, J.R. & Volk, D.W. Cortical parvalbumin interneurons and cognitive dysfunction in schizophrenia. *Trends Neurosci.* **35**, 57–67 (2012).
7. van Vreeswijk, C. & Sompolinsky, H. Chaos in neuronal networks with balanced excitatory and inhibitory activity. *Science* **274**, 1724–1726 (1996).
8. van Vreeswijk, C. & Sompolinsky, H. Chaotic balanced state in a model of cortical circuits. *Neural Comput.* **10**, 1321–1371 (1998).
9. Gilman, J.P., Medalla, M. & Luebke, J.I. Area-specific features of pyramidal neurons-a comparative study in mouse and rhesus monkey. *Cereb. Cortex* bhw062 (2016).
10. DeNardo, L.A., Berns, D.S., DeLoach, K. & Luo, L. Connectivity of mouse somatosensory and prefrontal cortex examined with trans-synaptic tracing. *Nat. Neurosci.* **18**, 1687–1697 (2015).
11. Hooks, B.M. *et al.* Laminar analysis of excitatory local circuits in vibrissal motor and sensory cortical areas. *PLoS Biol.* **9**, e1000572 (2011).
12. Bandeira, F., Lent, R. & Herculano-Houzel, S. Changing numbers of neuronal and non-neuronal cells underlie postnatal brain growth in the rat. *Proc. Natl. Acad. Sci. USA* **106**, 14108–14113 (2009).
13. Frick, A., Feldmeyer, D. & Sakmann, B. Postnatal development of synaptic transmission in local networks of L5A pyramidal neurons in rat somatosensory cortex. *J. Physiol. (Lond.)* **585**, 103–116 (2007).
14. Oswald, A.M. & Reyes, A.D. Maturation of intrinsic and synaptic properties of layer 2/3 pyramidal neurons in mouse auditory cortex. *J. Neurophysiol.* **99**, 2998–3008 (2008).
15. Oswald, A.M. & Reyes, A.D. Development of inhibitory timescales in auditory cortex. *Cereb. Cortex* **21**, 1351–1361 (2011).
16. Citri, A. & Malenka, R.C. Synaptic plasticity: multiple forms, functions, and mechanisms. *Neuropsychopharmacology* **33**, 18–41 (2008).
17. Brunel, N. Dynamics of sparsely connected networks of excitatory and inhibitory spiking neurons. *J. Comput. Neurosci.* **8**, 183–208 (2000).
18. Markram, H. *et al.* Reconstruction and simulation of neocortical microcircuitry. *Cell* **163**, 456–492 (2015).
19. Goris, R.L., Movshon, J.A. & Simoncelli, E.P. Partitioning neuronal variability. *Nat. Neurosci.* **17**, 858–865 (2014).
20. Gur, M., Beylin, A. & Snodderly, D.M. Response variability of neurons in primary visual cortex (V1) of alert monkeys. *J. Neurosci.* **17**, 2914–2920 (1997).
21. Rust, N.C., Schultz, S.R. & Movshon, J.A. A reciprocal relationship between reliability and responsiveness in developing visual cortical neurons. *J. Neurosci.* **22**, 10519–10523 (2002).
22. Zohary, E., Shadlen, M.N. & Newsome, W.T. Correlated neuronal discharge rate and its implications for psychophysical performance. *Nature* **370**, 140–143 (1994).
23. Avermann, M., Tomm, C., Mateo, C., Gerstner, W. & Petersen, C.C. Microcircuits of excitatory and inhibitory neurons in layer 2/3 of mouse barrel cortex. *J. Neurophysiol.* **107**, 3116–3134 (2012).

24. Levy, R.B. & Reyes, A.D. Spatial profile of excitatory and inhibitory synaptic connectivity in mouse primary auditory cortex. *J. Neurosci.* **32**, 5609–5619 (2012).
25. Perin, R., Berger, T.K. & Markram, H. A synaptic organizing principle for cortical neuronal groups. *Proc. Natl. Acad. Sci. USA* **108**, 5419–5424 (2011).
26. Pfeffer, C.K., Xue, M., He, M., Huang, Z.J. & Scanziani, M. Inhibition of inhibition in visual cortex: the logic of connections between molecularly distinct interneurons. *Nat. Neurosci.* **16**, 1068–1076 (2013).
27. Lefort, S., Tomm, C., Floyd Sarria, J.C. & Petersen, C.C. The excitatory neuronal network of the C2 barrel column in mouse primary somatosensory cortex. *Neuron* **61**, 301–316 (2009).
28. Holmgren, C., Harkany, T., Svennenfors, B. & Zilberter, Y. Pyramidal cell communication within local networks of layer 2/3 of rat neocortex. *J. Physiol. (Lond.)* **551**, 139–153 (2003).
29. Markram, H., Lübke, J., Frotscher, M., Roth, A. & Sakmann, B. Physiology and anatomy of synaptic connections between thick tufted pyramidal neurones in the developing rat neocortex. *J. Physiol. (Lond.)* **500**, 409–440 (1997).
30. Renart, A. *et al.* The asynchronous state in cortical circuits. *Science* **327**, 587–590 (2010).
31. de la Rocha, J., Doiron, B., Shea-Brown, E., Josić, K. & Reyes, A. Correlation between neural spike trains increases with firing rate. *Nature* **448**, 802–806 (2007).
32. Gullo, F. *et al.* Orchestration of "presto" and "largo" synchrony in up-down activity of cortical networks. *Front. Neural Circuits* **4**, 11 (2010).
33. Soriano, J., Rodríguez Martínez, M., Tlusty, T. & Moses, E. Development of input connections in neural cultures. *Proc. Natl. Acad. Sci. USA* **105**, 13758–13763 (2008).
34. Wilson, N.R., Ty, M.T., Ingber, D.E., Sur, M. & Liu, G. Synaptic reorganization in scaled networks of controlled size. *J. Neurosci.* **27**, 13581–13589 (2007).
35. Ivenshitz, M. & Segal, M. Neuronal density determines network connectivity and spontaneous activity in cultured hippocampus. *J. Neurophysiol.* **104**, 1052–1060 (2010).
36. Reyes, A. *et al.* Target-cell-specific facilitation and depression in neocortical circuits. *Nat. Neurosci.* **1**, 279–285 (1998).
37. Roxin, A., Brunel, N., Hansel, D., Mongillo, G. & van Vreeswijk, C. On the distribution of firing rates in networks of cortical neurons. *J. Neurosci.* **31**, 16217–16226 (2011).
38. Buzsáki, G. & Mizuseki, K. The log-dynamic brain: how skewed distributions affect network operations. *Nat. Rev. Neurosci.* **15**, 264–278 (2014).
39. Churchland, M.M. *et al.* Stimulus onset quenches neural variability: a widespread cortical phenomenon. *Nat. Neurosci.* **13**, 369–378 (2010).
40. Litwin-Kumar, A. & Doiron, B. Slow dynamics and high variability in balanced cortical networks with clustered connections. *Nat. Neurosci.* **15**, 1498–1505 (2012).
41. Okun, M. & Lampl, I. Instantaneous correlation of excitation and inhibition during ongoing and sensory-evoked activities. *Nat. Neurosci.* **11**, 535–537 (2008).
42. Xue, M., Atallah, B.V. & Scanziani, M. Equalizing excitation-inhibition ratios across visual cortical neurons. *Nature* **511**, 596–600 (2014).
43. Graupner, M. & Reyes, A.D. Synaptic input correlations leading to membrane potential decorrelation of spontaneous activity in cortex. *J. Neurosci.* **33**, 15075–15085 (2013).
44. Turrigiano, G.G., Leslie, K.R., Desai, N.S., Rutherford, L.C. & Nelson, S.B. Activity-dependent scaling of quantal amplitude in neocortical neurons. *Nature* **391**, 892–896 (1998).
45. Maffei, A., Nelson, S.B. & Turrigiano, G.G. Selective reconfiguration of layer 4 visual cortical circuitry by visual deprivation. *Nat. Neurosci.* **7**, 1353–1359 (2004).
46. Ullian, E.M., Sapperstein, S.K., Christopherson, K.S. & Barres, B.A. Control of synapse number by glia. *Science* **291**, 657–661 (2001).
47. Stellwagen, D. & Malenka, R.C. Synaptic scaling mediated by glial TNF-alpha. *Nature* **440**, 1054–1059 (2006).

ONLINE METHODS

Primary neuron cultures and expression of channelrhodopsin. Dissociated cortical neurons from postnatal (P0–P1) mice were prepared as described previously[48] and in accordance with guidelines of the New York University Animal Welfare Committee. Briefly, the mouse cortex was dissected in cold CMF-HBSS (Ca^{2+} and Mg^{2+} free Hank's balanced salt solution containing 1 mM pyruvate, 15 mM HEPES, 10 mM $NaHCO_3$). The tissue was dissociated in papain (15 U/mL, Roche) containing 1 mM L-cysteine, 5 mM 2-amino-5-phosphonopentanoic acid and 100 U/ml DNase (DN25; Sigma) for 25 min. After enzymatic inactivation in CMF-HBSS containing 100 mg/mL BSA (A9418; Sigma) and 40 mg/mL trypsin inhibitor (T9253; Sigma), pieces were mechanically dissociated with a pipette. Cells concentration was measured before plating using a hemocytometer. Approximately $0.2–3 \times 10^6$ cells were plated on each coverslip, resulting in a density of ~50–1,000 cells/mm^2 at the time of experiment. Neurons were seeded onto German glass coverslips (25 mm, #1 thickness, Electron Microscopy Science). Glass was cleaned in 3 N HCl for 48 h and immersed in sterile aqueous solution of 0.1 mg/mL poly-L-lysine (MW: 70,000–150,000; Sigma) in 0.1 M borate buffer for 12 h. Neurons were grown in Neurobasal medium (supplemented with B27, Glutamax and penicillin/streptomycin cocktail; Invitrogen) in a humidified incubator at 37 °C, 5% CO_2. One third of the culture medium was exchanged every 3 d.

Expression of channelrhodopsin (ChR2) in E neurons was achieved by crossing homozygote *Vglut2-Cre* mice (016963, Jackson Laboratory) with *ChR2*-loxP mice (Ai32, 012569, Jackson Laboratory). Alternatively, ChR2 expression was achieved by viral infection with AAV2-hSyn-hChR2(H134R)-mCherry of cortical neurons harvested from Swiss Webster wild-type mice (Jackson Laboratory). The virus was produced at 3×10^{12} cfu/mL by the University of North Carolina Vector Core Services using plasmid provided by Karl Deisseroth (Stanford University). At 3 d *in vitro* (DIV), the culture was infected with 1 μL of virus. Experiments were performed at 14–21 DIV, when neuronal characteristics and network connectivity were stable and expression of ChR2 was sufficient to enable reliable photostimulation.

Electrophysiological recordings. Recordings were performed at room temperature (20–25 °C) in artificial cerebrospinal fluid (aCSF) bubbled with 95% O_2 and 5% CO_2. The aCSF solution contained (in mM): 125 NaCl, 25 $NaHCO_3$, 25 D-glucose, 2.5 KCl, 2 $CaCl_2$, 1.25 NaH_2PO_4 and 1 $MgCl_2$. An alternative aCSF solution, in which 10 mM HEPES replaced the equivalent concentration of $NaHCO_3$, was also used to avoid perfusion during the experiment. Electrodes, pulled from borosilicate pipettes (1.5 OD) on a Flaming/Brown micropipette puller (Sutter Instruments), had resistances in the range of 6–10 MΩ when filled with internal solution containing (in mM): 130 κ-gluconate, 10 HEPES, 10 phosphocreatine, 5 KCl, 1 $MgCl_2$, 4 ATP-Mg and 0.3 mM GTP. In some experiments, 5 mM QX-314 was added to block the action potentials internally.

Cells were visualized through a 10× water-immersion objective using infrared differential interference contrast (IR-DIC) and fluorescence microscopy (BX51, Olympus). Simultaneous whole-cell current-clamp recordings were made from up to 4 neurons using BVC-700A amplifiers (Dagan). The signal was filtered at 5 kHz and digitized at 25 kHz using an 18-bit interface card (PCI-6289, National Instruments). Signal generation and acquisition were controlled by a custom user interface programmed with Labview (National Instruments).

Analysis of intrinsic and network properties of cortical cultures. For every experiment, IR-DIC images around the region of recording were saved for offline examination using a custom user interface programmed with Labview (National Instruments). Neuronal cultures can have local variations in their densities. Thus, cell density was determined locally by counting somata on a ~1×1 mm^2 area around the recording site. In **Figures 3b,c, 4c,d,g** (and **Supplementary Fig. 9a**) and **5b**, data were pooled according to densities. Low, medium and high densities corresponded to networks of neuronal densities (in neurons/mm^2): density < 200, 200 < density < 450 and 450 < density, respectively.

Intrinsic properties (**Supplementary Table 1** and **Supplementary Fig. 1**) were characterized by applying 15 current steps (−0.1 to +0.5 nA). The subthreshold membrane (input resistance, membrane time constant) and suprathreshold firing (spike threshold, spike width, after-hyperpolarization, rheobase, maximum firing rate) were measured using standard protocols programmed in Matlab (Mathworks).

To characterize postsynaptic potentials (PSPs), paired recordings were made from two neurons. Brief (20 ms; 0.1–0.4 nA) suprathreshold current pulses were delivered to one cell and the PSP (if connected) was measured in the other cell. The PSP parameters (E or I, magnitude, time-to-peak) were documented (**Supplementary Table 2**). By performing many paired recordings and documenting the distance between cell somata, the connection probability (P_c = number of connections/total tested) spatial profile (**Supplementary Fig. 2**) could be determined. The data points were grouped into 250 μm bins and the spatial profile fitted with a Gaussian function:

$$P_c(x) = p_0 \cdot \exp(-x^2 / 2\sigma^2) \tag{1}$$

where p_0 is peak probability, σ represents the spread of connectivity and x is the distance from the center.

In **Figure 1b**, data were first pooled according to density to compute the connection profile for each density. Then, the number of connections K plotted in **Figure 1c** was calculated by integration. The number of neurons contained in the annulus between x and $x + dx$ is

$$N(x) = \text{density} \cdot 2\pi x \cdot dx \tag{2}$$

The number of connections is then computed by summing the number of connected neurons in this annulus over space:

$$K = \int_0^{+\infty} N(x) \cdot P_c(x) = \text{density} \cdot \sigma^2 2\pi p_0 \tag{3}$$

Note that we use infinite boundaries, which might appear unrealistic because axons have finite lengths. However, the Gaussian shape of the connection profile ensures that the integral rapidly converges, such that the contribution of long-distance connections is minimal (for example, limiting the integration to $x = 1,500$ μm reduced K by only 5%).

We used a bootstrap procedure to estimate the s.d. of calculated K. For each density, we randomly subsampled 50% of the data, fitted the resulting profile as above (equation (1)), and computed the expected number of connections (equation (3)). This procedure was repeated 200 times to obtain an estimate for the mean and the s.d. of the distribution (**Fig. 1c**).

Optical stimulation setup. A digital light processing projector (DLP LightCrafter; Texas Instruments) was used to stimulate optically neurons expressing ChR2. The projector had a resolution of 608 × 684 pixels. The image of the projector was demagnified and collimated using a pair of achromatic doublet lenses (35 mm and 200 mm; Thorlabs; **Fig. 2b**). A dual-port intermediate unit (U-DP, Olympus) containing a 510 nm dichroic mirror (T510LPXRXT, Chroma) was placed between the fluorescent port and the projection lens. The resulting pixel size at the sample plane was a rectangle of dimensions 2.2 μm × 1.1 μm. The blue LED of the projector, with 460 nm center wavelength, was used to stimulate the ChR2-expressing neurons.

The CCD camera (C8484, Hamamatsu) was used to calibrate the light intensity as follows. The short-pass dichroic mirror was replaced with a half-reflecting mirror and a 100% reflecting mirror was placed at the sample plane. This allowed measurement of the light intensity at the point of stimulation and at other regions to estimate the contrast ratio. This is an important measure because it provides an estimate of the light intensity that a nonstimulated neuron receives during stimulation of the ChR2 expressing neurons. There are two common methods of measuring contrast. The full-on, full-off method measures the averaged brightness of a white test pattern and a black test pattern and expresses the two measurements as a ratio of white to black. The measured ratio was 815:1, close to the 685:1 ratio specified by the manufacturer. The ANSI contrast measurement uses a checkerboard pattern composed of 16 rectangles, eight white and eight black. The contrast ratio is then defined as the quotient of the averaged white pixels to the averaged black pixels. The ANSI contrast was 21:1 (compared to the 43:1 value provided by the manufacturer), which gives a lower bound for the contrast ratio. To get an insight of the real contrast ratio during experiment (specifically, to measure background illumination of our system), we measured the contrast ratio when a single region of interest was illuminated or when 20 areas were simultaneously illuminated. We found values of 700:1 and 170:1, respectively. During experiments, we used a light intensity of 10 mW/mm^2, which was calibrated with the camera and confirmed with a light power meter. Thus, we estimated the background light intensity to lie between 10 and 50 μW/mm^2 during photostimulation, which would give rise

to photocurrent of about 8–32 pA. This value, while insufficient to elicit spikes, could nevertheless generate postsynaptic potentials on the order of 0.1 to 1 mV. We therefore recorded neurons that either did not express ChR2 or whose dendritic processes did not overlap with the stimulated cells, to avoid any spurious correlation with the stimulus. However, note that the largest estimate of background stimulation is only relevant when neurons are synchronously activated.

Images were streamed continuously at a rate of 1,440 Hz from the computer to the projector via a graphic card (01G-P3-1526-KR; EVGA) using the HDMI port. We also measured the light intensity at the output of the projector using a photodiode (TSL13T; Texas Advanced Optoelectronics Solutions Inc.). We used this signal as an accurate trigger for synchronizing photostimulation and electrophysiological recordings offline.

Stimulation and recordings protocols. The cultured network was optically stimulated as follows. After identifying the fluorescent ChR2-expressing neurons, a subset of these neurons were designated for photostimulation with regions of interest or ROIs that surrounded their somata (**Fig. 2a**). Typically, 15–60 ROIs were used, so that about 10% of neurons in the field were stimulated. A 3- to 5-s train of brief light pulses (5 ms) was delivered to the neurons in each ROI.

Although the sequence of light pulses could be generated using a Poisson process, we opted to use noise-driven leaky-integrate-and-fire (LIF) neuron models instead. With the appropriate parameters, the use of LIF models minimized the occurrences of closely spaced spikes, which would cause failure in ChR2 activation (**Supplementary Fig. 5**). The LIF model has a membrane time constant $\tau_m = 60$ ms and input resistance $R_m = 300$ MΩ. The input current to each unit was a sum of a time varying $I_k(t)$ and a constant I_{cst} component so that $V_k(t)$ obeys

$$\tau_m \dot{V}_k(t) = -V_k(t) + R_m(I_{cst} + I_k(t)) \tag{4}$$

A spike was generated when V_k exceeded the voltage threshold $V_t = -50$ mV and was then reset to $V_{reset} = -65$ mV. The initial condition was $V_k(t_0) = -60$ mV. Given the parameters mentioned here and the statistics of the noisy current input $I_k(t)$ (see below), the generated spike trains had an average firing rate $\nu_{stim} \approx 4.8$ Hz and a Fano factor of ~1. The large membrane time constant and the refractory period, $t_{ref} = 10$ ms, eliminated high-frequency bursts. The stimulus rate ν_{stim} was modulated by varying the constant input current I_{cst}.

The input current obeys the following equation (see **Supplementary Fig. 4**):

$$I_k(t) = \sqrt{C_{stim}} \cdot I_{com}(t) + \sqrt{1 - C_{stim}} \cdot I_{ind,k}(t) \tag{5}$$

where $I_{com}(t)$ is a noisy input common to all stimulated neurons, $I_{ind,k}(t)$ is an independent noisy input to each neuron k, and C_{stim} is a constant. Because $I_{com}(t)$ and $I_{ind,k}(t)$ have the same variance and are independent random variables, the cross-correlation coefficient between two input currents $I_k(t)$ and $I_l(t)$ converges to C_{stim} for long time series:

$$C_{stim} = \frac{\langle I_k(t) \cdot I_l(t) \rangle_t}{\sqrt{\langle I_k(t)^2 \rangle_t \cdot \langle I_l(t)^2 \rangle_t}} \tag{6}$$

where $\langle \cdot \rangle_t$ denotes average over time. The spatial cross-correlation C_{stim} ('stimulus correlation') was varied between 0 and 1 (in steps of 0.25). The resulting spike correlation, measured as the Pearson correlation of the firing rates, also varies between 0 and 1 (**Supplementary Fig. 4b**). However, because this measure depends on the count window, we used the current correlation C_{stim} to refer to stimulus correlation in the main text.

$I_{com}(t)$ and $I_{ind,k}(t)$ were realizations of a Gaussian (Ornstein-Uhlenbeck) noise process and were generated using

$$I(t_{n+1}) = I(t_n) \cdot e^{-dt/\tau} + \sigma \cdot \sqrt{1 - e^{-2dt/\tau}} \cdot \xi(t_n) \tag{7}$$

where $I(t_0) = 0$ is the initial condition, $\sigma = 24$ pA is the s.d., $\tau = 50$ ms is the correlation time, and $\xi(t_n)$ is a random variable drawn from the standard normal distribution of zero mean and unity variance.

During data collection, the stimuli (with specified ν_{stim} and C_{stim}) were delivered 5–6 times if subthreshold potentials were recorded in whole-cell mode and 10–30 times if spikes were recorded in cell-attached mode. At least 5 s separated each stimulation.

Data analyses. As observed in other *in vitro* studies in cultures[49] or in slices[43], spontaneous network-wide bursts occurred. Spontaneous, correlated bursts have also been observed *in vivo*[50–52] indicating that they are not artifacts of the *in vitro* preparation. Under the conditions of the experiments, these bursts were infrequent (~1–2 bursts/minute) and were readily identified based on their long-duration (≳ 1 s) high-frequency spikes or depolarization and by the fact that they were observed simultaneously in all the recording electrodes. These events were excluded from the analysis as they represented a different activity regime[43] of debated origin (for example, ref. 53–55). The theoretical implications of these bursts are beyond the scope of the paper and are currently under active investigation.

Analysis of spike data. The spike rate was defined as the number of spikes divided by the stimulation period. To estimate spike correlation, spikes were first binned at d$t = 1$ ms. The firing rate $r_i^n(t)$ of neuron i for the nth realization ($n \in \{1..N_{trials}\}$) was computed by convolving the spike count with a Gaussian kernel of width $t = 50$ ms. The average firing rate $\tilde{r}_i(t)$ over the various trials of the same stimulation protocol was defined as: $\tilde{r}_i(t) = \langle r_i^n(t) \rangle_n$, where $\langle \cdot \rangle_n$ denotes average over trials.

The spike correlation coefficient between neuron i and neuron j was estimated as the Pearson coefficient between $\tilde{r}_i(t)$ and $\tilde{r}_j(t)$ during the stimulation period. The spike count Fano factor was calculated as the variance of spike count in a 500-ms time window (or other lengths; **Supplementary Fig. 8**) divided by the mean. This quantity was computed across trials before being averaged over time. Very sparsely firing neurons (rate < 0.1 Hz) were excluded from this analysis.

Analysis of membrane potential data. The membrane potential V of neuron i for the nth realization ($n \in \{1..N_{trials}\}$) is denoted as $V_i^n(t)$. We define signal as the average response $\tilde{V}_i(t)$ over the various trials of the same stimulation protocol:

$$\tilde{V}_i(t) = V_i^n(t)_n \tag{8}$$

The average depolarization (or hyperpolarization) was defined as the difference between the mean membrane potential during external stimulation and its value at rest (**Fig. 4c,f,h** and **Supplementary Figs. 9, 11** and **12**). The s.d. during evoked activity was measured as the s.d. of the membrane potential computed during the stimulation period (**Fig. 4d,f,h** and **Supplementary Figs. 9, 11** and **12**). This value was then averaged across trials.

We calculated the zero-lag correlation coefficient between membrane potentials of neurons recorded simultaneously (**Figs. 5b–d** and **6c,d** and **Supplementary Fig. 12**). We defined the signal correlation as the correlation between the membrane potentials $\tilde{V}_i(t)$ of neuron 1 and neuron 2 averaged over trials as

$$r_{V_1,V_2}^{signal} = \frac{\left\langle \left(\tilde{V}_1(t) - \overline{\tilde{V}_1}\right) \cdot \left(\tilde{V}_2(t) - \overline{\tilde{V}_2}\right) \right\rangle_t}{\sqrt{\sigma_{\tilde{V}_1} \sigma_{\tilde{V}_2}}} \tag{9}$$

where $\overline{\tilde{V}_i} = \langle \tilde{V}_i(t) \rangle_t$ is the average over time.

Additionally, we defined the noise response of neuron i as the deviation of a given trial n from the mean response:

$$V_{noise,i}^n(t) = V_i^n(t) - \left\langle V_i^n(t) \right\rangle_n \tag{10}$$

Similarly, the noise correlation between neurons 1 and neuron 2 is defined by the following:

$$r_{V_1,V_2}^{noise} = \left\langle \frac{\left\langle \left(V_{noise,1}^n(t) - \overline{V}_{noise,1}^n\right) \cdot \left(V_{noise,1}^n(t) - \overline{V}_{noise,2}^n\right) \right\rangle_t}{\sqrt{\sigma_{V_{noise,1}^n} \sigma_{V_{noise,2}^n}}} \right\rangle_n \tag{11}$$

Noise correlation was thus computed for each trial and then averaged across trials.

Statistical analysis. Data collection and analysis were not performed blind to the conditions of the experiments. No randomization method was used to collect data and no data points or animals were excluded. All the data were shown as mean ± s.e.m., unless stated otherwise. Two group comparisons were performed using either paired or unpaired two-sided Mann-Whitney *U*-test. Firing rates that had long-tail distributions were first log-transformed before being compared.

A generalized linear regression model with Bonferroni correction was performed when more than two groups were compared. The variances between groups were assumed to be different. No statistical methods were used to predetermine sample sizes.

A **Supplementary Methods Checklist** is available.

Data availability. The data that support the findings of this study are available from the corresponding author upon reasonable request.

Code availability. Data acquisition (Labview) and analysis (Labview or Matlab) software used in this paper are described in Online Methods and will be available upon reasonable request.

48. Hilgenberg, L.G. & Smith, M.A. Preparation of dissociated mouse cortical neuron cultures. *J. Vis. Exp.* **562**, 562 (2007).
49. Wagenaar, D.A., Pine, J. & Potter, S.M. An extremely rich repertoire of bursting patterns during the development of cortical cultures. *BMC Neurosci.* **7**, 11 (2006).
50. Leinekugel, X. *et al.* Correlated bursts of activity in the neonatal hippocampus in vivo. *Science* **296**, 2049–2052 (2002).
51. Chiu, C. & Weliky, M. Spontaneous activity in developing ferret visual cortex in vivo. *J. Neurosci.* **21**, 8906–8914 (2001).
52. Weliky, M. & Katz, L.C. Correlational structure of spontaneous neuronal activity in the developing lateral geniculate nucleus in vivo. *Science* **285**, 599–604 (1999).
53. Eytan, D. & Marom, S. Dynamics and effective topology underlying synchronization in networks of cortical neurons. *J. Neurosci.* **26**, 8465–8476 (2006).
54. Orlandi, J.G., Soriano, J., Alvarez-Lacalle, E., Teller, S. & Casademunt, J. Noise focusing and the emergence of coherent activity in neuronal cultures. *Nat. Phys.* **9**, 582–590 (2013).
55. Feinerman, O., Segal, M. & Moses, E. Identification and dynamics of spontaneous burst initiation zones in unidimensional neuronal cultures. *J. Neurophysiol.* **97**, 2937–2948 (2007).